



## Computational Studies on the Structure, NBO, HOMO-LUMO analysis of 1-Benzylimidazole based on density functional theory studies

S.Jaya<sup>1</sup>, B. Raja<sup>2</sup>, K.Anitha<sup>3</sup> and V. Balachandran<sup>4</sup><sup>1</sup>Department of Physics, Periyar EVR College (Autonomous), Tiruchirappalli- 620 023, India.<sup>2</sup>Department of Physics, Government Arts College, Kulithalai- 639 120, Karur, India.<sup>3</sup>Department of Physics, Bharathidasan University constituent college, Lalgudi, Tiruchirappalli 621 601, India.<sup>4</sup>Department of Physics, A. A. Government Arts College, Musiri- 621 211, India.

### ARTICLE INFO

#### Article history:

Received: 8 May 2015;

Received in revised form:

20 June 2015;

Accepted: 25 June 2015;

#### Keywords

1-Benzylimidazole,  
Vibrational spectra,  
NBO,  
HOMO-LUMO,  
MEP surface.

### ABSTRACT

The solid phase FTIR and FT-Raman spectra of 1-Benzylimidazole (BI) have been recorded in the regions 4000–400 cm<sup>-1</sup> and 3500–100 cm<sup>-1</sup>, respectively. The optimized geometry, frequency and intensity of the vibrational bands, NBO analysis, HOMO- LUMO study of BI in DFT levels of theory using B3LYP/6-31G and B3LYP/6-311+G basis set. The harmonic vibrational frequencies were calculated and the scaled values have been compared with experimental FTIR and FT-Raman spectra. A detailed interpretation of the vibrational spectra of the title compound has been made on the basis of the calculated potential energy distribution (PED). Stability of the molecule arising from hyperconjugative interactions leading to its bioactivity, charge delocalization have been analyzed using natural bond orbital (NBO) analysis. The calculated HOMO-LUMO energies shows that charge transfer occur within the molecule. The observed and calculated frequencies are found to be in good agreement.

© 2015 Elixir All rights reserved.

### Introduction

Imidazole and its derivatives have received a great deal of interest from spectroscopists owing to their strong cardiotoxic [1], analgesic [2], anti-inflammatory [3,4] and antimicrobial activities [5–8]. Imidazole nucleus forms the building block of some well known components of human organisms, i.e. the amino acid histidine, vitamin B12, a component of DNA base structure and purines, histamine and biotin. It is also present in the structure of many natural synthetic drug molecules, e.g. cimetidine, azomycin and metronidazole [9]. They are also used in many drugs as an inducer of phase I and II enzymes with wide spectrum detection of precarcinogen in short-term bioassays, hepatic levels of cytochrome P-450 (CYP) and mutagenic activation of various carcinogens [10]. Their inhibitory properties against the replication of polioviruses, adenosine deaminase, and casein kinase have been well demonstrated [11]. Some attempts were made for the interpretations of the vibrational spectra of imidazole derivatives [12]. Literature survey reveals that to the best of our knowledge, the results based on Quantum chemical calculations, FT-IR and FT-Raman spectral analyses on 1-Benzylimidazole (BI) have no reports. Here we reported detailed interpretations of the infrared and Raman spectra based on the theoretical results, which are acceptable and supportable to each other. In the present work, we have attempted to interpret the vibrational spectra of BI by using B3LYP level of theory throughout with the 6-31G and 6-311+G, basis sets are implemented in the Gaussian 09 program suite [13].

### Experimental method

BI was provided by Lancaster Chemical Company, UK, which is of spectroscopic grade and hence used for recording the spectra as such without any further purifications. The room temperature Fourier Transform infrared spectrum of BI was

measured in the 4000-400cm<sup>-1</sup> region at a resolution of ± 1cm<sup>-1</sup> using BRUKER IFS-66V FT-IR Spectrometer equipped with a KBr pellets were used in the spectral measurements. The FT-Raman spectrum was recorded on a BRUKER IFS-66V model interferometer equipped with an FRA -106 FT-Raman accessory in the 3500-100 cm<sup>-1</sup> Stokes region using the 1064nm line of a Nd:YAG laser for excitation operating at 200mW power.

### Computational details

Analysis of molecular geometry optimizations, energy, and vibrational frequencies was carried out with the Gaussian 09 software package [14] at the DFT (B3LYP) levels supplemented with the standard 6-31G and 6-311+G basis sets. Cartesian representation of the theoretical force constants has been computed at optimized geometry. Vibrational modes were assigned by means of visual inspection using the GAUSSVIEW [15] program. Data revealed that DFT calculations using a basis set incorporating polarized functions yielded results that are in better agreement with the experimental data. For the plots of simulated IR and Raman spectra, pure Lorentzian band shapes were used with a band width of ±1 cm<sup>-1</sup>. Prediction of Raman intensities was carried out by the following procedure. The Raman activities (S<sub>i</sub>) calculated by the Gaussian 09 program were converted to relative Raman intensities (I<sub>i</sub>) using the following relationship derived from the basic theory of scattering.

$$I_i = \frac{f(\nu_0 - \nu_i)^4 S_i}{\nu_i [1 - \exp(-\frac{hc\nu_i}{kt})]} \dots\dots\dots (1)$$

where  $\nu_0$  is the exciting wavenumber (cm<sup>-1</sup> units)  $\nu_i$  is the vibrational wavenumber of the i<sup>th</sup> normal mode, h, c and k are universal constant and f is a suitably chosen common normalization factor for all peak intensities.

Natural bond orbital analysis (NBO) was also performed by the Gaussian 09 W program at the B3LYP level of theory analysis transforms the canonical delocalized Hartree-Fock (HF) Molecular orbital's (MO) into localized MOs that are closely tied to chemical bonding concepts. This process involves sequential transformation of non-orthogonal atomic orbital's (AOs) to the sets of Natural atomic orbital's (NAOs), Natural hybrid orbital's (NHOs) Natural bond orbital's (NBOs). The localized basis sets are completely described the wave functions in the most economic method, as electron density and other properties that are described by the minimum amount of filled NBO. The interaction between filled and anti-bonding (or) Rydberg orbital's represented the deviation of the molecule from the Lewis structure and be used as the measure of delocalization. This non-covalent bonding anti-bonding charge transfer interactions can be quantitatively described in terms of the second order perturbation interaction energy ( $E^{(2)}$ ) [16-19].

## Results and discussion

### Molecular geometry

The molecular structure of a BI along with numbering of atoms is shown in Fig. 1. The maximum number of potentially active observable fundamentals of a non-linear molecule that contains N atoms is equal to  $(3n-6)$ , apart from three translational and three rotational degrees of freedom [20]. NALPA having 22 atoms with 60 Normal modes of vibrations which are distributed amongst the symmetry species as  $(3N-6)_{\text{vib}}=41A' + 19A''$  (in-plane) + 19 $A''$  (out-of-plane). The  $A'$  vibrations are totally symmetric and give rise to polarized Raman lines whereas  $A''$  vibrations are antisymmetric and give rise to depolarized Raman lines. The observed and simulated spectra of the title compound are shown in Fig 2 and 3 respectively.

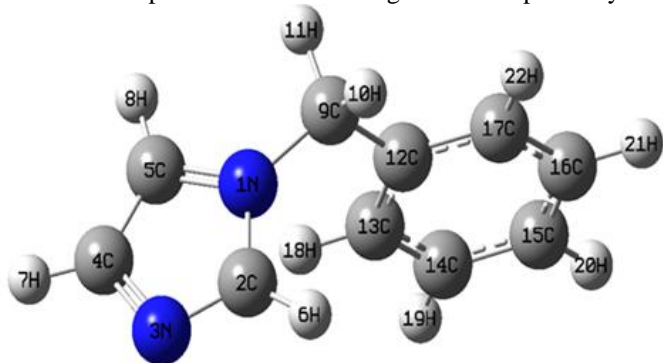


Fig 1. Optimized geometrical structure and atomic labeling of 1-Benzylimidazole

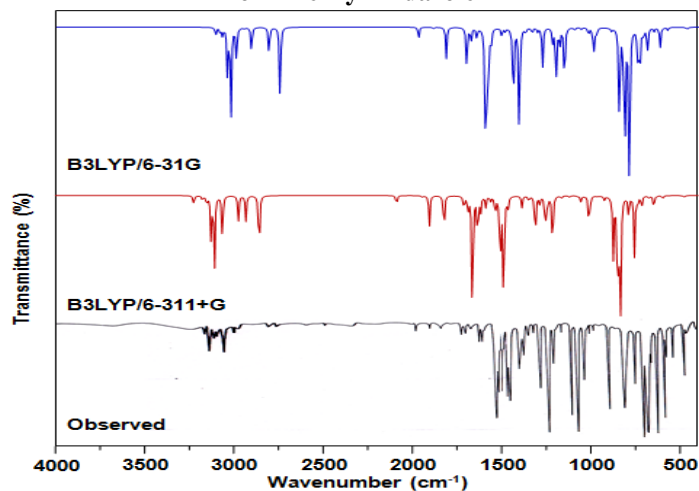
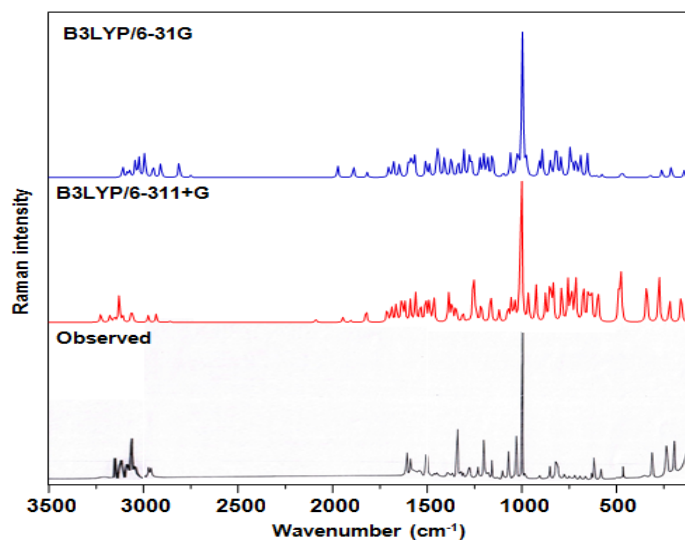


Fig 2. Observed FT-IR and simulated spectrum of 1-Benzylimidazole



Normal coordinate analysis was carried out to provide a complete assignment of the fundamental vibrational frequencies for the molecule. For this purpose the full set of standard internal coordinates are listed in Table 1. From these a redundant set of local symmetry coordinates was constructed by suitable linear combinations of internal coordinates following the recommendations of Fogarasi and Puly et al.[21-23] and are given in Table 2. The theoretically calculated force fields were transformed to this later set of vibrational co-ordinates and are used in all subsequent calculations. The most optimized geometrical parameters (bond length, bond angle and dihedral angle) were also calculated by B3LYP/6-31G and B3LYP/6-311+G basis sets, which are depicted in Table 3.

### Vibrational assignments

The detailed vibrational analysis of fundamental modes of BI along with the FT-IR and FT-Raman experimental frequencies and the unscaled and scaled vibrational frequencies using B3LYP/6-31G and B3LYP/6-311+G basis sets are presented in Table 4.

### C-H vibrations

Aromatic compounds commonly exhibit multiple weak bands in the region 3100–3000  $\text{cm}^{-1}$  due to aromatic C-H stretching vibrations [24–27]. The bands appeared at 3090, 3068, 3045, 3022, 3000, 2954, 2908  $\text{cm}^{-1}$  in FT-IR spectrum and 3091, 3070, 2952  $\text{cm}^{-1}$  in FT-Raman spectrum are assigned to C-H ring stretching vibrations. The band identified at 3225, 3176, 3153, 3128, 3109, 3065, 3057, 2975  $\text{cm}^{-1}$  in B3LYP/6-31G and 3085, 3072, 3044, 3025, 2994, 2950, 2910  $\text{cm}^{-1}$  in B3LYP/6-311+G methods are assigned to C-H ring stretching vibrations. The C-H in-plane and out-of-plane bending vibrations generally lie in the range 1000–1300  $\text{cm}^{-1}$  and 950–800  $\text{cm}^{-1}$  [28,29], respectively. In the present case, eight C-H in-plane bending vibrations of the title compound identified at 1508, 1489, 1387, 1348, 1312, 1287, 1256, 1038  $\text{cm}^{-1}$  in B3LYP/6-31G and 1445, 1412, 1340, 1270, 1282, 1225, 1206, 1002  $\text{cm}^{-1}$  in B3LYP/6-311+G methods are assigned to C-H in-plane bending vibrations. The C-H out-of-plane bending vibrations are observed at 979, 831, 738, 626, 614  $\text{cm}^{-1}$  in FT-IR spectrum and 910, 853, 819, 614  $\text{cm}^{-1}$  in FT-Raman spectrum. According to the literature, the in-plane and out-of-plane bending vibrations are found to be lower than their characteristic regions due to the substitution of the  $\text{CH}_2$ .

### $\text{CH}_2$ Vibrations

For the assignments of  $\text{CH}_2$  group frequencies, basically six fundamentals can be associated to each  $\text{CH}_2$  group namely,  $\text{CH}_2\text{ss}$  (symmetric stretch);  $\text{CH}_2\text{ass}$  (asymmetric stretch);  $\text{CH}_2\text{sciss}$  (scissoring) and  $\text{CH}_2$  rock (rocking) which belongs to

in-plane vibrations. In addition to that, CH<sub>2</sub>wag (wagging) and CH<sub>2</sub> twist group would be expected to be depolarized for out-of-plane symmetry species. Here, the title molecule BI under consideration possesses one CH<sub>2</sub> group give rise to 6 fundamental modes of vibration. The anti symmetric CH<sub>2</sub> stretching vibrations are generally observed in the regions 3100–3000 cm<sup>-1</sup> respectively; while the symmetric stretch will appear between 3000 and 2900 cm<sup>-1</sup>. The calculated CH<sub>2</sub> asymmetric vibrations were identified at 2933 cm<sup>-1</sup> in B3LYP/6-31G and 2812 cm<sup>-1</sup> in B3LYP/6-311+G methods and symmetric vibrations are found at 2859 in B3LYP/6-31G and 2750 cm<sup>-1</sup> in B3LYP/6-311+Gmethod. According to the literature, the stretching vibrations are found to be lower than their characteristic regions due to the substitution of the CH<sub>2</sub>, benzene group. The bands corresponding to scissoring, wagging, rocking and twisting vibrations of CH<sub>2</sub> groups are summarized in Table 4. These assignments are also supported by literature data as well as computed harmonics [30].

### CC Vibrations

The position and intensity of ring stretching vibrations depend on the nature of the ring and the type of substitution. In BI, FT-IR bands at 1976, 1895, 1825, 1686, 1512, 1375cm<sup>-1</sup> and FT-Raman bands at 1506, 1456, 1368, 1182 cm<sup>-1</sup> have been assigned to aromatic CC stretching vibrations. The ring in-plane and out of plane bending vibrations are assigned in the characteristic regions. The ring stretching vibrations are all coupled vibrations, some vibrations coupled with C-H bending and some with C-CH<sub>2</sub> bending and some with C-C-N stretching vibrations. Small changes due to the changes in force constant/reduced mass ratio resulting mainly due to the extent of mixing between ring and substituent group [31]. The absorption involves stretching of bands in the ring and interaction between these stretching.

### C–N vibrations

The identification of C–N, C=N vibrations is a difficult task, since the mixing of vibrations is possible in this region. Silverstein et al. [32] assigned the C–N stretching vibrations in the range 1382–1266 cm<sup>-1</sup> for aromatic amines. In the present work, the bands observed at 1651, and 1605 cm<sup>-1</sup> in FT-IR spectrum and 1582 cm<sup>-1</sup> in FT-Raman spectrum are assigned to C–N stretching vibrations. The theoretically computed value of C–N, C=N stretching vibrations also falls in the region 1689,1644, 1635 cm<sup>-1</sup> and 1650, 1600, 1586 cm<sup>-1</sup> by both B3LYP/6-31G and B3LYP/6-311+G methods, and the vibrations are found to be higher than their characteristic regions. This is indicating that the impact of substitution CH<sub>2</sub> group in the molecule influence the vibration of aromatic C–H.

### NBO analysis

Natural bond orbital analysis gives the accurate possible natural Lewis structure picture of  $\Phi$  because all orbital are mathematically chosen to include the highest possible percentage of the electron density. Interaction between both filled and virtual orbital spaces was correctly explained by the NBO analysis and it could enhance the analysis of intra- and intermolecular interactions. The second-order Fock matrix was carried out to evaluate donor (i)–acceptor (j) i.e. interaction between donor-level bonds and acceptor-level bonds in the NBO analysis [33], The result of interaction is a loss of occupancy from the concentration of electron NBO of the idealized Lewis structure into an empty non-Lewis orbital. For each donor (i) and acceptor (j), the stabilization energy  $E^{(2)}$  associates with the delocalization  $i \rightarrow j$  is follows:

$$E^{(2)} = \Delta E_y = q_i \frac{F(i, j)^2}{\epsilon_j - \epsilon_i} \dots \dots \dots (2)$$

Where  $q_i$  is the donor orbital occupancy, are  $\epsilon_j$  and  $\epsilon_i$  are diagonal elements and  $F(i, j)$  is the off-diagonal NBO Fock matrix element. A natural bond orbital analysis provide an efficient method for studying intra- and intermolecular bonding and interaction between bonds, and also provides a convenient basis for investigating charge transfer or conjugative interaction in molecular systems. Some electron donor orbital, acceptor orbital, and the interacting stabilization energy resulted from second-order perturbation theory are reported [34]. The larger the  $E^{(2)}$  value the more intensive the interaction between electron donors and electron acceptor, i.e., the more donation tendency from electron donors to electron acceptors and the greater the extent of conjugation of the whole system [35]. Delocalization of electron density between occupied Lewis type (bond or lone pair) NBO orbitals and formally unoccupied (antibond or Rydberg) non-Lewis NBO orbital corresponds to a stabilizing donor–acceptor interaction. NBO analysis has been performed on BI at the B3LYP/6-311G level in order to elucidate the intramolecular rehybridization and delocalization of electron density within the molecule.

The most important interactions in BI having lone pair LP (1) N<sub>3</sub> with that of anti bonding N<sub>1</sub>–C<sub>2</sub>, results in the stabilization of 6.86 kJ/mol, which denotes larger delocalization. The maximum energy transfer occurs from LP (1) N<sub>1</sub> to C<sub>2</sub>–N<sub>3</sub> (44.67 kJ/mol), respectively, as shown in Table 5.

### HOMO-LUMO

The conjugated molecules are characterized by a highest occupied molecular orbital-lowest unoccupied molecular orbital (HOMO–LUMO) separation, which is the result of a significant degree of intermolecular charge transfer (ICT) from the end-capping electron-donor to the efficient electron acceptor group through p conjugated path. The strong charge transfer interaction through p conjugated bridge results in substantial ground state donor–acceptor mixing and the appearance of a charge transfer band in the electronic absorption spectrum. Therefore, an electron density (ED) transfer occurs from the more aromatic part of the p conjugated system in the electron-donor side to electron-withdrawing part. The aromatic orbital components of the frontier molecular orbitals are shown in Fig. 4. The HOMO–LUMO energy gap value are found at -0.19784 a.u in B3LYP/6-311+G. The calculated ground state energy of BI is -0.21596 a.u in B3LYP method, which are responsible for the title compound. [36]

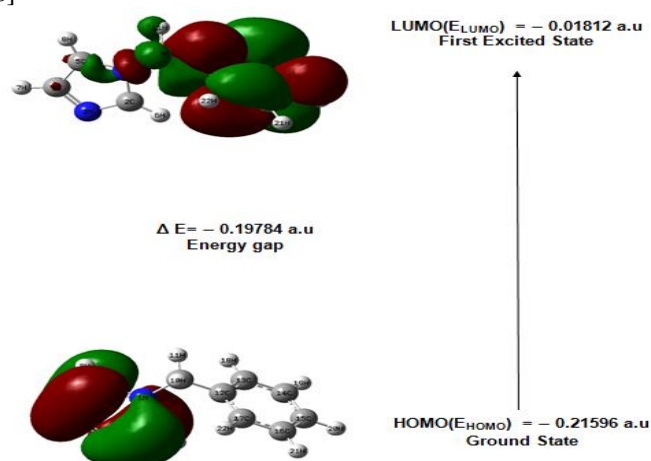


Fig 4. The atomic orbital composition of the molecular orbital for 1-Benzylimidazole

Table 1. Definition of internal coordinates of 1-Benzylimidazole

No	Symbol	Type	Definition
Stretching			
1-8	$p_i$	C-C	$C_{12}-C_{13}, C_{13}-C_{14}, C_{14}-C_{15}, C_{15}-C_{16}, C_{16}-C_{17}, C_{17}-C_{12}, C_9-C_{12}, C_4-C_5$
9-16	$q_i$	C-H	$C_{13}-H_{18}, C_{14}-H_{19}, C_{15}-H_{20}, C_{16}-H_{21}, C_{17}-H_{22}, C_4-H_7, C_5-H_8, C_2-H_6$
17-18	$q_i$	C-H(metheline)	$C_9-H_{10}, C_9-H_{11}$
19-23	$r_i$	C-N	$C_9-N_1, C_2-N_1, C_2-N_3, C_4-N_3, C_5-N_1$
In-plane bending			
24-29	$\alpha_i$	C-C-C(Ring)	$C_{12}-C_{13}-C_{14}, C_{13}-C_{14}-C_{15}, C_{14}-C_{15}-C_{16}, C_{15}-C_{16}-C_{17}, C_{16}-C_{17}-C_{12}, C_{17}-C_{12}-C_{13}$
30-31	$\alpha_i$	C-C-C	$C_{13}-C_{12}-C_9, C_{17}-C_{12}-C_9$
32-41	$\beta_i$	C-C-H	$C_{12}-C_{13}-H_{18}, C_{14}-C_{13}-H_{18}, C_{13}-C_{14}-H_{19}, C_{15}-C_{14}-H_{19}, C_{14}-C_{15}-H_{20}, C_{16}-C_{15}-H_{20}, C_{15}-C_{16}-H_{21}, C_{17}-C_{16}-H_{21}, C_{16}-C_{17}-H_{22}, C_{12}-C_{17}-H_{22}$
42-43	$\beta_i$	C-C-H	$C_{12}-C_9-H_{10}, C_{12}-C_9-H_{11}$
44	$\gamma_i$	H-C-H	$H_{10}-C_9-H_{11}$
45-49	$\alpha_i$	Ring	$N_1-C_2-N_3, C_2-N_3-C_4, N_3-C_4-C_5, C_4-C_5-N_1, C_5-N_1-C_2$
50-53	$\delta_i$	N-C-H	$N_1-C_2-H_6, N_3-C_2-H_6, N_3-C_4-H_7, N_1-C_5-H_8$
54	$\beta_i$	C-C-H	$H_7-C_4-C_5$
55	$\beta_i$	C-C-H	$C_4-C_5-H_8$
56-57	$\pi_i$	C-N-C	$C_9-N_1-C_5, C_9-N_1-C_2$
58-59	$\delta_i$	N-C-H	$N_1-C_9-H_{10}, N_1-C_9-H_{11}$
Out-of-plane bending			
60-65	$\omega_i$	C-C-C-C(Ring)	$C_{12}-C_{13}-C_{14}-C_{15}, C_{13}-C_{14}-C_{15}-C_{16}, C_{14}-C_{15}-C_{16}-C_{17}, C_{15}-C_{16}-C_{17}-C_{12}, C_{16}-C_{17}-C_{12}-C_{13}, C_{17}-C_{12}-C_{13}-C_{14}$
66-70	$\omega_i$	C-C-C-H	$C_{12}-C_{13}-C_{14}-H_{18}, C_{13}-C_{14}-C_{15}-H_{19}, C_{14}-C_{15}-C_{16}-H_{20}, C_{15}-C_{16}-C_{17}-H_{21}, C_{16}-C_{17}-C_{12}-H_{22}$
71-72	$\omega_i$	C-C-C-H	$H_{10}-C_9-C_{12}-C_{17}(C_{13}), H_{11}-C_9-C_{12}-C_{17}(C_{13})$
73-77	$\omega_i$	Ring	$N_1-C_2-N_3-C_4, C_2-N_3-C_4-C_5, N_3-C_4-C_5-N_1, C_4-C_5-N_1-C_2, C_5-N_1-C_2-N_3$
78-80	$\omega_i$	C-N	$H_6-C_2-N_1-N_3, H_7-C_4-C_5-N_3, H_8-C_5-C_4-N_1$
81	$\omega_i$	C-C-H-H	$C_{12}(N_1)-C_9-H_{10}-H_{11}$
82	$\omega_i$	C-C-C-N	$C_{13}-C_{12}-C_9-N_1$

Table 2. Definition of Local Symmetry coordinates of 1-Benzylimidazole

No	Symbol	Definition
1-8	C-C	$p_1, p_2, p_3, p_4, p_5, p_6, p_7, p_8$
9-16	C-H	$q_9, q_{10}, q_{11}, q_{12}, q_{13}, q_{14}, q_{15}, q_{16}$
17	$CH_{2(ss)}$	$q_{17}+q_{18}$
18	$CH_{2(ass)}$	$q_{17}-q_{18}$
19-23	C-N	$r_{19}, r_{20}, r_{21}, r_{22}, r_{23}$
In-plane bending		
24	$R_{trigd}$	$(\alpha_{24}-\alpha_{25}+\alpha_{26}-\alpha_{27}+\alpha_{28}-\alpha_{29})/\sqrt{6}$
25	$R_{symmetric}$	$(-\alpha_{24}-\alpha_{25}+2\alpha_{26}-\alpha_{27}-\alpha_{28}-2\alpha_{29})/\sqrt{12}$
26	$R_{asymmetric}$	$(\alpha_{24}-\alpha_{25}+\alpha_{26}-\alpha_{27})/2$
27	bCC	$(\alpha_{30}-\alpha_{31})/\sqrt{2}$
28-32	bCH	$(\beta_{32}-\beta_{33})/\sqrt{2}, (\beta_{34}-\beta_{35})/\sqrt{2}, (\beta_{36}-\beta_{37})/\sqrt{2}$
	bCH	$(\beta_{38}-\beta_{39})/\sqrt{2}, (\beta_{40}-\beta_{41})/\sqrt{2}$
33	$bCH_{2rock}$	$(\beta_{42}-\beta_{43})/\sqrt{2}$
34	$bCH_{2twist}$	$(\beta_{42}+\beta_{43})/\sqrt{2}$
35	$bCH_{2sciss}$	$(2\gamma_{44}-\beta_{42}-\beta_{43})/\sqrt{6}$
36	Ring 1	$\alpha_{45}+a(\alpha_{46}+\alpha_{49}), b(\alpha_{47}-\alpha_{48})$
37	Ring 2	$(a-b)(\alpha_{46}-\alpha_{49})+(1-a)(\alpha_{47}-\alpha_{48})$
38-39	bCH	$(\delta_{50}-\delta_{51})/\sqrt{2}, (\delta_{52}-\beta_{53})/\sqrt{2}$
40	bCH	$(\beta_{54}-\beta_{55})/\sqrt{2}$
41-42	bNC	$\pi_{56}, \pi_{57}$
43	bNCH	$(\delta_{58}-\delta_{59})/\sqrt{2}$
Out-of-plane bending		
44	$\omega R_{trigd}$	$(\omega_{60}-\omega_{661}+\omega_{62}-\omega_{63}+\omega_{64}+\omega_{65})/\sqrt{6}$
45	$\omega R_{symmd}$	$(\omega_{60}-\omega_{62}+\omega_{64}-\omega_{65})/2$
46	$\omega R_{asymmd}$	$(-\omega_{60}+2\omega_{61}-\omega_{62}-\omega_{63}+2\omega_{64}-\omega_{65})/\sqrt{12}$
47-51	$\omega CH$	$\omega_{66}, \omega_{67}, \omega_{68}, \omega_{69}, \omega_{70}$
52-53	$\omega CH$	$\omega_{71}, \omega_{72}$
54	$\omega Ring$	$b(\omega_{73}+\omega_{77})+a(\omega_{74}+\omega_{76})+\omega_{75}$
55	$\omega Ring$	$(a-b)(\omega_{77}-\omega_{73})+(1-a)(\omega_{76}-\omega_{74})$
56-58	$\omega CN$	$\omega_{78}, \omega_{79}, \omega_{80}$
59	$\omega CH_{2twist}$	$\omega_{80}$
60	$\omega CN$	$\omega_{81}$

Table 3. Optimized geometrical parameters of 1-Benzylimidazole by B3LYP/6-31G and B3LYP/6-311+G

Parameters	Bond length		Parameters	Bond angle		Parameters	Dihedral angle	
	B3LYP/ 6-31G	B3LYP/ 6-311+G		B3LYP/ 6-31G	B3LYP/ 6-311+G		B3LYP/ 6-31G	B3LYP/ 6-311+G
N1-C2	1.38	1.38	C2-N1-C5	106.75	106.75	C5-N1-C2-N3	-0.21	0.07
N1-C5	1.39	1.39	C2-N1-C9	126.64	126.67	C5-N1-C2-H6	179.55	-179.98
N1-C9	1.47	1.47	C5-N1-C9	126.58	126.58	C9-N1-C2-N3	-178.63	179.76
C2-N3	1.33	1.33	N1-H22-N3	111.54	111.58	C9-N1-C2-H6	1.13	-0.05
C2-H6	1.08	1.08	N1-C2-H6	126.61	122.61	C2-N1-C5-C4	0.16	-0.04
N3-C4	1.40	1.40	N3-C2-H6	125.85	125.81	C2-N1-C5-H8	179.60	-179.31
C4-C5	1.37	1.37	C2-N3-C4	105.56	105.48	C9-N1-C5-C4	178.58	-179.73
C4-H7	1.08	1.07	N3-C4-C5	110.20	110.18	C9-N1-C5-H8	-1.98	1.00
C5-H8	1.08	1.07	N3-C4-H7	121.14	121.09	C2-N1-C9-H10	-49.18	-7.45
C9-H10	1.10	1.09	C5-C4-H7	128.65	128.73	C2-N1-C9-H11	-163.78	-122.28
C9-H11	1.10	1.09	N1-C5-C4	105.94	106.01	C2-N1-C9-H12	73.80	114.44
C9-C12	1.52	1.52	N1-C5-H8	121.79	121.88	C5-N1-C9-H10	132.71	172.17
C12-C13	1.40	1.40	C4-C5-H8	132.26	132.11	C5-N1-C9-H11	18.11	57.35
C12-C17	1.40	1.40	N1-C9-H10	108.57	106.56	C5-N1-C9-H12	-104.32	-65.94
C13-C14	1.40	1.40	N1-C9-H11	106.82	108.96	N1-C2-N3-C4	0.18	-0.07
C13-H18	1.09	1.08	N1-C9-H12	114.64	114.18	H6-C2-N3-C4	-179.58	179.73
C14-C15	1.40	1.40	H10-C9-H11	106.60	106.74	C2-N3-C4-C5	-0.07	0.04
C14-H19	1.09	1.08	H10-C9-C12	109.74	110.19	C2-N3-C4-H7	-179.75	-179.91
C15-C16	1.40	1.40	H11-C9-C12	110.33	109.90	N3-C4-C5-N1	-0.06	0.00
C15-H20	1.09	1.08	C9-C12-C13	121.59	121.30	N3-C4-C5-H8	-179.42	179.16
C16-C17	1.40	1.40	C9-C12-C17	119.29	119.66	H7-C4-C5-N1	179.59	179.95
C16-H21	1.09	1.08	C13-C12-C17	119.09	119.02	H7-C4-C5-H8	0.22	-0.89
C17-H22	1.09	1.08	C12-C13-C14	120.32	120.40	N1-C9-C12-C13	32.33	-36.49
			C12-C13-H18	119.68	119.70	N1-C9-C12-C17	149.64	145.44
			C14-C13-H18	119.99	119.89	H10-C9-C12-C13	154.66	83.88
			C13-C14-C15	120.30	120.27	H10-C9-C12-C17	-27.31	-96.49
			C13-C14-H19	119.65	119.69	H11-C9-C12-C13	-88.17	-159.27
			C15-C14-H19	120.04	120.04	H11-C9-C12-C17	89.86	22.66
			C14-C15-H16	119.66	119.65	C9-C12-C13-C14	177.86	-177.78
			C14-C15-H20	120.18	120.16	C9-C12-C13-H18	-2.87	3.01
			C16-C15-H20	120.17	120.18	C17-C12-C13-C14	-0.18	0.30
			C15-C16-C17	120.03	120.02	C17-C12-C13-H18	-179.10	-178.91
			C15-C16-H21	120.16	120.16	C9-C12-C17-C16	177.63	177.63
			C17-C16-H21	119.82	119.81	C9-C12-C17-H22	2.59	-2.56
			C12-C17-C16	120.60	120.63	C13-C12-C17-C16	0.45	-0.48
			C12-C17-H22	119.67	119.72	C13-C12-C17-H22	-179.33	179.33
			1C6-C17-H22	119.72	119.65	C12-C13-C14-C15	-0.18	0.06
						C12-C13-C14-H19	179.65	-179.80
						H18-C13-C14-C15	-179.45	179.27
						H18-C13-C14-H19	0.38	-0.59
						C13-C14-C15-C16	0.26	-0.24
						C13-C14-C15-H20	179.90	-179.89
						H19-C14-C15-C16	-179.57	179.62
						H19-C14-C15-H20	0.07	-0.03
						C14-C15-C16-C17	0.02	0.06
						C14-C15-C16-H21	179.47	-179.51
						H20-C15-C16-C17	-179.62	179.71
						H20-C15-C16-H21	-0.17	0.14
						C15-C16-C17-H22	179.40	-179.51
						H21-C16-C17-H12	-179.83	179.88

**Table 4. vibrational assignments of fundamental observed frequencies and calculated frequencies of 1-Benzylimidazole using by B3LYP/6-31G and B3LYP/6-311+G**

Mode No.	Symmetry Species	Observed frequencies		Calculated frequencies				Vibrational assignments / (%)
		FT-IR	FT-Raman	Unscaled		Scaled		
				B3LYP/6-31G	B3LYP/6-311+G	B3LYP/6-31G	B3LYP/6-311+G	
1	A'		3114	3322	3284	3225	3110	νCH(98)
2	A'	3090	3091	3307	3260	3176	3085	νCH(98)
3	A'	3068	3070	3297	3258	3153	3072	νCH(98)
4	A'	3045	-	3227	3194	3128	3044	νCH(98)
5	A'	3022	-	3215	3182	3109	3025	νCH(98)
6	A'	3000	-	3206	3172	3065	2994	νCH(98)
7	A'	2954	2952	3196	3162	3057	2950	νCH(98)
8	A'	2908	-	3182	3150	2975	2910	νCH(98)
9	A''	2818	-	3100	3064	2933	2812	νCH <sub>2</sub> <sub>asym</sub> (98)
10	A'	2750	-	3058	3026	2859	2750	νCH <sub>2</sub> <sub>sym</sub> (97)
11	A'	1976	-	1665	1643	2089	1975	νCC(78), δCH(21)
12	A'	1895	-	1646	1623	1945	1892	νCC, (96)
13	A'	1825	-	1558	1544	1905	1820	νCC(59), δCH(28), δCH <sub>2</sub> <sub>sciss</sub> (24)
14	A'	1709	-	1542	1534	1823	1706	δCH <sub>2</sub> <sub>sciss</sub> (85)
15	A'	1686	-	1527	1516	1712	1682	νCC(65), δCN(18), δCH <sub>2</sub> <sub>sciss</sub> (10)
16	A'	1651	-	1516	1501	1689	1650	νCN(66), δCH(31)
17	A'	1605	-	1501	1489	1664	1600	νCN(63), δCH(30)
18	A'	-	1582	1420	1415	1635	1586	νCN(53), γCH(32), CH <sub>2</sub> <sub>wagg</sub> (12)
19	A''	1569	-	1407	1399	1618	1570	νCN(58), CH <sub>2</sub> <sub>twist</sub> (32)
20	A'	1512	1506	1384	1369	1589	1510	νCC(65), δCH(13)
21	A''	1490	-	1376	1360	1562	1491	νCN(65)
22	A'	-	1456	1347	1324	1536	1452	νCC, (45) νCN(24), CH <sub>2</sub> <sub>wagg</sub> (15)
23	A'	1443	-	1322	1310	1508	1445	δCH(44), ν CN(16), γCH(10)
24	V	1410	-	1260	1252	1489	1412	δCH(70)
25	A'	1375	1368	1238	1226	1465	1376	νCC(58), δCH(23)
26	A'	1342	1342	1233	1225	1387	1340	δCH(73)
27	A''	1308	1320	1224	1216	1369	1310	γCH <sub>2</sub> <sub>twist</sub> (65)
28	A'	1271	-	1215	1211	1348	1270	δCH(78)
29	A'	-	1285	1140	1127	1312	1282	δCH(78)
30	A'	1228	1228	1128	1115	1287	1225	δCH(78)
31	A'	1205	1205	1095	1082	1256	1206	δCH(65), δCN(30)
32	A'	-	1182	1067	1055	1243	1185	νCC (66), δCH(32)
33	A''	1160	1160	1046	1036	1215	1159	δRing <sub>1</sub> (75)
34	A'	-	1103	1037	1030	1165	1102	δRing <sub>2</sub> (68)
35	A'	1068	1069	1034	1027	1121	1065	δRing <sub>2</sub> (68)
36	A'	1035	-	1003	1009	1074	1032	δRing <sub>2</sub> (67)
37	A'	-	1021	999	998	1056	1025	δCH <sub>2</sub> <sub>rock</sub> (65)
38	A'	1000	1000	937	936	1038	1002	δCH(46), δCH <sub>2</sub> <sub>rock</sub> (26)
39	A'	-	990	925	924	1012	993	δRing <sub>1</sub> (68)
40	A''	979	-	886	891	1003	978	γCH(56), γRing(32)
41	A''	-	910	882	878	965	912	γCH(58), γRing(30)
42	A'	899	-	832	827	925	895	δCC(65),
43	A''	-	853	821	810	875	852	γCH, γRing(23)
44	A''	831	-	785	783	853	828	γCH, γRing(24)
45	A''	-	819	758	762	849	820	γCH(58)
46	A''	794	774	748	742	835	796	γRing <sub>2</sub> (68)
47	A''	-	751	725	714	789	750	γRing <sub>2</sub> (68)
48	A''	738	-	680	673	756	738	γCH(59)
49	A'	717	717	657	655	738	718	δCN(60), δCH(23)
50	A'	694	694	645	639	716	695	δCN(70)
51	A'	660	660	594	593	675	658	δCN(72)
52	A''	626	-	478	478	648	624	γCH(60)
53	A''	614	614	424	420	633	610	γCH(58)
54	A''	580	580	340	344	598	581	γCH <sub>2</sub> <sub>rock</sub> (63)
55	A''	478	-	328	323	487	479	γCN(58)
56	A''	467	465	249	245	475	468	γCC(56)
57	A''	-	328	199	202	340	325	γRing <sub>2</sub> (55)
58	A''	-	260	72	74	275	264	γCN(55)
59	A''	-	214	40	44	219	215	γCN(54)
60	A''	-	146	16	21	158	146	γRing <sub>1</sub> (55)

A': In-plane; A'': out-of-plane; sym: symmetric stretching; asym: asymmetric stretching; ν: stretching; δ: in-plane bending; γ: out-of-plane bending; τ: torsion; wagg: wagging; sciss: scissoring; τ: twisting; sb: symmetric bonding; ipb: in-plane-bending; opb: out-plane-bending; ipr: in-plane-rocking; opr: out-plane-rocking;

Table 5. Second-order perturbation theory analysis of Fock matrix in NBO basic corresponding to the intra molecular bonds of 1-Benzylimidazole

Donor (i)	ED (i) (e)	Acceptor (j)	ED (j) (e)	<sup>a</sup> E <sup>(2)</sup> (kJ mol <sup>-1</sup> )	<sup>b</sup> E(j) – E(i) (a.u.)	<sup>c</sup> F(i,j) (a.u.)
σ(N <sub>1</sub> -C <sub>2</sub> )	1.98809	σ*(C <sub>5</sub> -H <sub>8</sub> )	0.01009	2.59	1.29	0.052
σ(N <sub>1</sub> -C <sub>5</sub> )	1.98456	σ*(C <sub>2</sub> -H <sub>6</sub> )	0.01226	2.55	1.28	0.051
σ(N <sub>1</sub> -C <sub>9</sub> )	1.98943	σ*(C <sub>12</sub> -C <sub>13</sub> )	0.02538	1.81	0.77	0.037
σ(C <sub>2</sub> -N <sub>3</sub> )	1.98508	σ*(N <sub>1</sub> -C <sub>9</sub> )	0.03955	3.73	1.06	0.057
π(C <sub>2</sub> -N <sub>3</sub> )	1.85391	σ*(C <sub>4</sub> -C <sub>5</sub> )	0.01829	21.28	0.28	0.073
σ(C <sub>2</sub> -H <sub>6</sub> )	1.98587	σ*(N <sub>1</sub> -C <sub>5</sub> )	0.01955	2.71	0.97	0.046
σ(N <sub>3</sub> -C <sub>4</sub> )	1.98542	σ*(C <sub>2</sub> -H <sub>6</sub> )	0.01226	3.09	1.24	0.055
σ(C <sub>4</sub> -C <sub>5</sub> )	1.98793	σ*(N <sub>1</sub> -C <sub>9</sub> )	0.03955	4.39	0.37	0.059
π(C <sub>4</sub> -C <sub>5</sub> )	1.83729	σ*(C <sub>2</sub> -N <sub>3</sub> )	0.00948	18.15	0.24	0.063
σ(C <sub>4</sub> -H <sub>7</sub> )	1.98738	π*(C <sub>2</sub> -N <sub>3</sub> )	0.41093	2.60	1.00	0.045
σ(C <sub>5</sub> -H <sub>8</sub> )	1.98820	σ*(N <sub>1</sub> -C <sub>2</sub> )	0.03822	2.66	0.97	0.046
σ(C <sub>9</sub> -H <sub>10</sub> )	1.97734	σ*(C <sub>12</sub> -C <sub>13</sub> )	0.02538	3.52	1.11	0.056
σ(N <sub>9</sub> -C <sub>11</sub> )	1.97976	σ*(C <sub>12</sub> -C <sub>17</sub> )	0.02561	3.93	1.11	0.059
σ(C <sub>9</sub> -H <sub>12</sub> )	1.97506	σ*(N <sub>1</sub> -C <sub>5</sub> )	0.01955	3.02	1.08	0.051
σ(C <sub>12</sub> -H <sub>13</sub> )	1.97303	σ*(C <sub>12</sub> -C <sub>17</sub> )	0.02561	4.31	1.27	0.066
π(C <sub>12</sub> -H <sub>13</sub> )	1.65998	σ*(C <sub>19</sub> -C <sub>17</sub> )	0.32915	20.133	0.28	0.067
σ(C <sub>12</sub> -C <sub>17</sub> )	1.97271	π*(C <sub>12</sub> -C <sub>13</sub> )	0.35429	4.27	1.28	0.066
σ(C <sub>13</sub> -C <sub>14</sub> )	1.97903	σ*(C <sub>12</sub> -C <sub>13</sub> )	0.02538	3.34	1.27	0.055
σ(C <sub>13</sub> -H <sub>18</sub> )	1.98208	σ*(C <sub>12</sub> -C <sub>17</sub> )	0.02561	4.25	1.09	0.061
σ(C <sub>14</sub> -C <sub>15</sub> )	1.97993	σ*(C <sub>13</sub> -C <sub>14</sub> )	0.01599	2.82	1.27	0.054
π(C <sub>14</sub> -C <sub>15</sub> )	1.65566	π*(C <sub>16</sub> -C <sub>17</sub> )	0.32915	21.03	0.27	0.068
σ(C <sub>14</sub> -H <sub>19</sub> )	1.98261	σ*(C <sub>12</sub> -C <sub>13</sub> )	0.02538	3.64	1.09	0.056
σ(C <sub>15</sub> -C <sub>16</sub> )	1.97994	σ*(C <sub>16</sub> -C <sub>17</sub> )	0.01587	2.86	1.27	0.054
σ(C <sub>15</sub> -C <sub>20</sub> )	1.98248	σ*(C <sub>13</sub> -C <sub>14</sub> )	0.01559	3.59	1.09	0.056
σ(C <sub>16</sub> -C <sub>17</sub> )	1.97879	σ*(C <sub>9</sub> -C <sub>12</sub> )	0.02150	3.46	1.14	0.054
π(C <sub>16</sub> -C <sub>17</sub> )	1.66384	π*(C <sub>12</sub> -C <sub>13</sub> )	0.35429	21.64	0.28	0.070
σ(C <sub>16</sub> -H <sub>21</sub> )	1.98259	σ*(C <sub>12</sub> -C <sub>17</sub> )	0.02561	3.66	1.09	0.056
σ(C <sub>17</sub> -H <sub>22</sub> )	1.98188	σ*(C <sub>12</sub> -C <sub>13</sub> )	0.02538	4.27	1.10	0.061
LP(1)N1	1.54405	π*(C <sub>2</sub> -N <sub>3</sub> )	0.41093	44.67	0.25	0.096
LP(1)N3	1.93995	σ*(N <sub>1</sub> -C <sub>2</sub> )	0.03822	6.86	0.75	0.064

<sup>a</sup>E<sup>(2)</sup> means energy of hyperconjugative interactions.

<sup>b</sup> Energy difference between donor and acceptor *i* and *j* NBO orbitals.

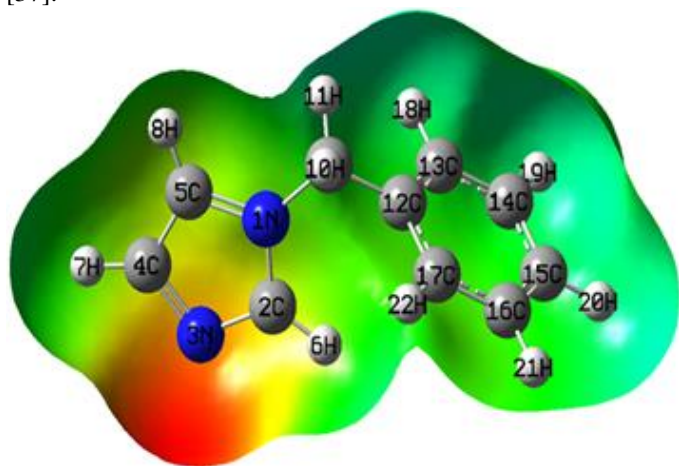
<sup>c</sup>F(*i*,*j*) is the Fock matrix element between *i* and *j* NBO orbitals.

Table 6. Thermo dynamical parameters of BID calculated at B3LYP/6-311+G

Thermo dynamical parameter	Values
Zero-point vibrational energy(kcal/Mol)	113.45992
Zero-point correction (hatee/particle)	0.180810
Thermal correction to energy	0.190241
Thermal correction to enthalpy	0.191185
Thermal correction to Gibbs free energy	0.143726

### Molecular electrostatic potential

Molecular electrostatic potential (MEP) at a point in the space around a molecule gives an indication of the net electrostatic effect produced at that point by the total charge distribution (electron + nuclei) of the molecule and correlates with dipole moments, electronegativity, partial charges and chemical reactivity of the molecules. It provides a visual method to understand the relative polarity of the molecule. An electron density isosurface mapped with electrostatic potential surface depicts the size, shape, charge density and site of chemical reactivity of the molecules. The different values of the electrostatic potential represented by different colors; red represents the regions of the most negative electrostatic potential, blue represents the regions of the most positive electrostatic potential and green represents the region of zero potential. Potential increases in the order red < orange < yellow < green < blue. Such mapped electrostatic potential surface have been plotted for title molecule in B3LYP/6-311+G basis set using the computer software Gauss view. Projections of these surfaces along the molecular plane and a perpendicular plane are given in Fig. 5. This figure provides a visual representation of the chemically active sites and comparative reactivity of atoms [37].



**Fig 5. DFT B3LYP/6-311+G calculated 3D molecular electrostatic potential of 1-Benzylimidazole**

### Thermodynamic parameters

In addition to the vibrational assignments, several thermodynamic parameters, rotational constants, and dipole moment have been presented in Table 6. The self consistent field (SCF) energy, zero point vibrational energies (ZPVEs), rotational constants and entropy  $S_{vib}(T)$  are calculated to the extent of accuracy and variations in the ZPVEs seem to be insignificant [38]. Dipole moment reflects the molecular charge distribution and is given as a vector in three dimensions. Therefore, it can be used as descriptor to depict the charge movement across the molecule. Direction of the dipole moment vector in a molecule depends on the centers of positive and negative charges. Dipole moments are strictly determined for neutral molecules. For charged systems, its value depends on the choice of origin and molecular orientation.

### Conclusion

The present investigation thoroughly analyzed the HOMO–LUMO, NBO analyses, and the vibrational spectra, both infrared and Raman of BI molecule with B3LYP/6-31G and B3LYP/6-311+G methods. All the vibrational bands observed in the FT-IR and FT-Raman spectra of the compound are assigned to the various modes of vibration and most of the modes have wavenumbers in the expected range. The complete vibrational assignments of wave numbers are made on the basis of potential

energy distribution (PED). The scaled B3LYP/6-311+G results are the best over the B3LYP/6-31G method. The molecular electrostatic potential surfaces (MEP) together with complete analysis of the vibrational spectra, both IR and Raman spectra help to identify the structural properties of the title molecule. The excellent agreement of the calculated and observed vibrational spectra reveals the advantages of higher basis set for quantum chemical calculations. NBO analysis provides an efficient method for studying inter and intra molecular interaction in molecular system. The stabilization energy has been calculated from second order perturbation theory. Natural Bond Orbital analysis shows the differences in interaction of energies are due to the substitution of  $\text{CH}_2$  group. Finally, the calculated HOMO and LUMO energies show that charge transfer occur in the molecule, which are responsible for the bioactive property of the biomedical compound BI

### References

- [1] R.S. Tuttle, C. Garcia-Minor, M. Simon, *J. Pharmacol. Exp. Ther.* 194 (1975) 624.
- [2] D. Davison, M. Weiss, M. Jelling, *J. Org. Chem.* 2 (1934) 319.
- [3] H. Schubert, W.V. Berg, H. Andrea, *Math-Naturwiss. Reihe* 11 (1962) 603.
- [4] Y. Mori, J. Tsuji, *Tetrahedron* 27 (1971) 4039–4042.
- [5] D.M. James, H.M. Gills, *Human Antiparasitic Drug: Pharmacology and Usage*, Wiley, New York, 1996.
- [6] C. Delescluse, M.P. Piechock, N. Ledirac, R.H. Hines, R. Li, X. Gidrol, R. Rahmani, *Biochem. Pharmacol.* 61 (2001) 399–407.
- [7] V.L. Miller, C.J. Gloud, E.C. Sonka, R.N. Jensial, *J. Agric. Food. Chem.* 21 (1973) 931.
- [8] K.K. Monthilal, C. Karunakaran, A. Rajendiran, R. Murugesan, *J. Inorg. Biochem.* 98 (2004) 322–332.
- [9] U. Ucucu, N.G. Karaburun, I. Isikdag, *Il Farmaco* 56 (2001) 285–290.
- [10] Y. Mori, A. Koide, K. Fuwa, Y. Kobayashi, *Mutagenesis* 16 (2001) 479–486.
- [11] A.E. Ledesma, J. Zinzuk, J.J. Lopez Gonzalez, A. Ben Altabef, S.A. randan, *J. Mol. Struct.* 924–926 (2009) 322–331.
- [12] C. James, C. Ravikumar, V.S. Jayakumar, I. Hubert Joe, *J. Raman Spectroscop.* 40 (2009) 537–545.
- [13] M. J. Frisch, G. W. Trucks, H. B. Schlegel, G. E. Scuseria, M. A. Robb, J. R. Cheesman, V.G. Zakrzewski, J. A. Montgomery, Jr., R. E. Strtmann, J. C. Burant, S. Dapprich, J. M. Milliam, A. D. Daniels, K. N. Kudin, M. C. Strain, O. Farkas, J. Tomasi, V. Barone, M. Cossi, R. Camme, B. Mennucci, C. Pomelli, C. Adamo, S. Clifford, J. Ochterski, G.A. Petersson, P. Y. Ayala, Q. Cui, K. Morokuma, N. Rega, P. Salvador, J. J. Dannenberg, D. K. Malich, A. D. Rabuck, K. Raghavachari, J.B. Foresman, J. Cioslowski, J. V. Ortiz, A. G. Baboul, B. B. Stetanov, G. Liu, A. Liashenko, P. Piskorz, I. Komaromi, R. Gomperts, R. L. Martin, D. J. Fox, T. Keith, M. A. Al-Laham, C. Y. Peng, A. Nnsyskkara, M. Challacombe, P. M. W. Gill, B. Johnson, W. Chen, M.W. Wong, J. L. Andres, C. Gonzalez, M. Head-Gordon, E. S. Replogle and J. A. Pople, (2009) GAUSSIAN 09, Revision A.02, Gaussian, Inc., Pittsburgh.
- [14] M.J. Frisch, G.W. Trucks, H.B. Schlegel, G.E. Scuseria, M.A. Robb, et al., *Gaussian 09, Revision A. 02*, Gaussian Inc., Wallingford, CT, 2009.
- [15] A. Frisch, A.B. Niesen, A.J. Holder, *Gausses View Users Manual*, Gaussian Inc., 2008.

- [16] A.E. Reed, F. Weinhold, *J. Chem. Phys.* 83 (1985) 1736–1740.
- [17] M. Snehathatha, C. Ravi Kumar, I. Hubert Joe, V.S. Jaya Kumar, *J. Raman Spectrosc.* 40 (2009) 1121–1126.
- [18] I. Hubert Joe, I. Kostova, C. Ravi Kumar, M. Amalanathan, S.C. Pinzaru, *J. Raman Spectrosc.* 40 (2009) 1033–1038.
- [19] A.E. Ledesma, J. Zinzuk, A. Ben Altabef, J.J. Lopez Gonzalez, S.A. Brandan, *J. Raman Spectrosc.* 40 (2009) 1004–1010.
- [20] M. Silverstein, G. Clayton Basseler, C. Morill, *Spectrometric Identification of Organic Compound*, Wiley, New York, 1981.2560.
- [21] P. Pulay, G. Fogarasi, F. Pong, J.E. Boggs, *J. Amer. Chem. Soc.* 101 (1979) 2550–2560.
- [22] G. Fogarasi, X. Zhou, P.W Taylor, P. Pulay, *J. Am. Chem. Soc.* 114 (1992) 8191.
- [23] G. Fogarasi, P. Pulay, J.R. Durig, *Vib. Spectra Struct*, 14 (1995) 125.
- [24] V. Krishnakumar, V. Balachandran, T. Chithambarathanu, *Spectrochim. Acta, Part A* 62 (2005) 918–925.
- [25] N. Puviarasan, V. Arjunan, S. Mohan, *Turk. J. Chem.* 26 (2002) 323–334.
- [26] G. Varsanyi, *Vibrational Spectra of Benzene Derivatives*, Academic Press, New York, 1969.
- [27] V. Krishnakumar, R. John Xavier, *Indian J. Pure Appl. Phys.* 41 (2003) 597–602.
- [28] V. Krishnakumar, V.N. Prabavathi, *Spectrochim. Acta, Part A* 71 (2008) 449–457.
- [29] A. Altun, K. Golcuk, M. Kumru, *J. Mol. Struct.* 637 (2003) 155–169.
- [30] F.R. Dollish, W.G. Fateley, F.F. Bentley, *Characteristics Raman Frequencies of Organic Compounds*, John Wiley, New York, 1974.
- [31] Interpretation of Infrared spectra, in: R.A Meyers (Ed.), *A Practical Approach John Coates in Encyclopedia of Analytical Chemistry*, John Willey & Sons Ltd., Chichester, 2000.
- [32] R.M. Silverstein, R.M. Clayton Bassler, T.C. Morril, *Spectroscopic Identification of Organic Compounds*, John Wiley, New York, 1991.
- [33] M.Szafran, A. Komasa, E.B. Adamska, *J. Mol. Struct. (Theochem)* 827 (2007) 101.
- [34] C. James, A. Amal Raj, R. Reghunathan, I. Hubert Joe, V.S. Jayakumar, *J. Raman Spectrosc.* 37 (2006) 1381–1392.
- [35] Sebastian, N. Sundaraganesan, *Spectrochim. Acta* 75 (2010) 941–952.
- [36] D. Arul Dhas, I. Hubert Joe, S.D.D. Roy, T.H. Freeda, *Spectrochim. Acta, Part A* 77 (2010) 36–44.
- [37] V.P. Gupta, A. Sharma, V. Viridi, V.J. Ram, *Spectrochim. Acta, Part A* 64 (2006) 57–67.
- [38] P.B. NagabalaSubramanian, S. Periyandi, S. Mohan, *Spectrochim. Acta, Part A* 77 (2010) 150–159.